Electronic Supplementary Material (ESI) for Molecular Systems Design & Engineering.

Electronic Supplementary Information: Controlling the morphology of hybrid polymer/nanoparticles active layer of solar cell: mesoscopic simulation

Pavel Komarov, Pavel Baburkin, Viktor Ivanov, Show-An Chen and Alexei Khokhlov

Here we present additional computer simulation data on the morphologies of the systems (shown in Fig.4 in the paper), including snapshots and static structure factors, as well as simulation data on the chain conformations, i.e., on the gyration radius.

In Fig.ESI-1 we show the data on the average gyration radius, Rg, for the chains $C_{16}S_4$, $C_{14}S_6$, $C_{12}S_8$, $C_{10}S_{10}$ (indicated in the legend). The averaging was performed over all chains in each system as well as over several configurations of each system accumulated during the productive runs. The average error bar is shown in the center of the graph in order to keep a good visibility of data points. From these data we can conclude that there is almost no dependence on the content of copolymer chains and nanoparticles in the systems, but there is a quite pronounced dependence on the composition of copolymer chains, i.e., the chain size increases with increasing *n*/*N* ratio (*n* is the length of S-block, *N* is the length of copolymer chain). Such a trend is in agreement with the morphological changes observed in Fig.4 in this paper: in the lamellar morphology the copolymer chains are maximally extended, i.e., their gyration radius is larger than those in morphologies with cylindrical and spherical domains.

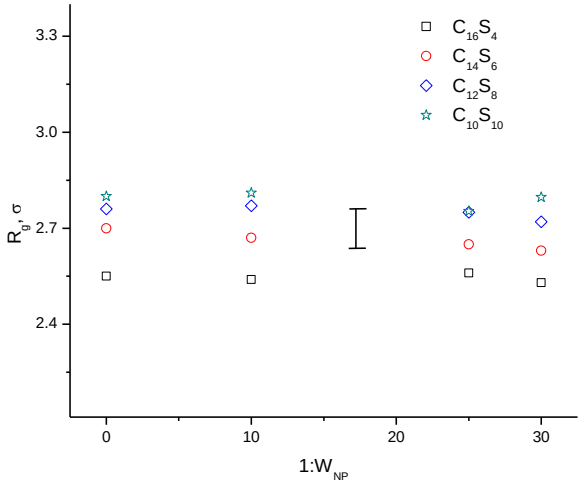

Figure ESI-1. Average gyration radius of chains in different systems (the composition of diblock-copolymers is indicated in the legend). The vertical segment in the center of the graph indicates the average error bar.

In Fig.ESI-2 we present better quality pictures of several morphologies used for construction of the state diagram shown in the Fig. 4 in the paper.

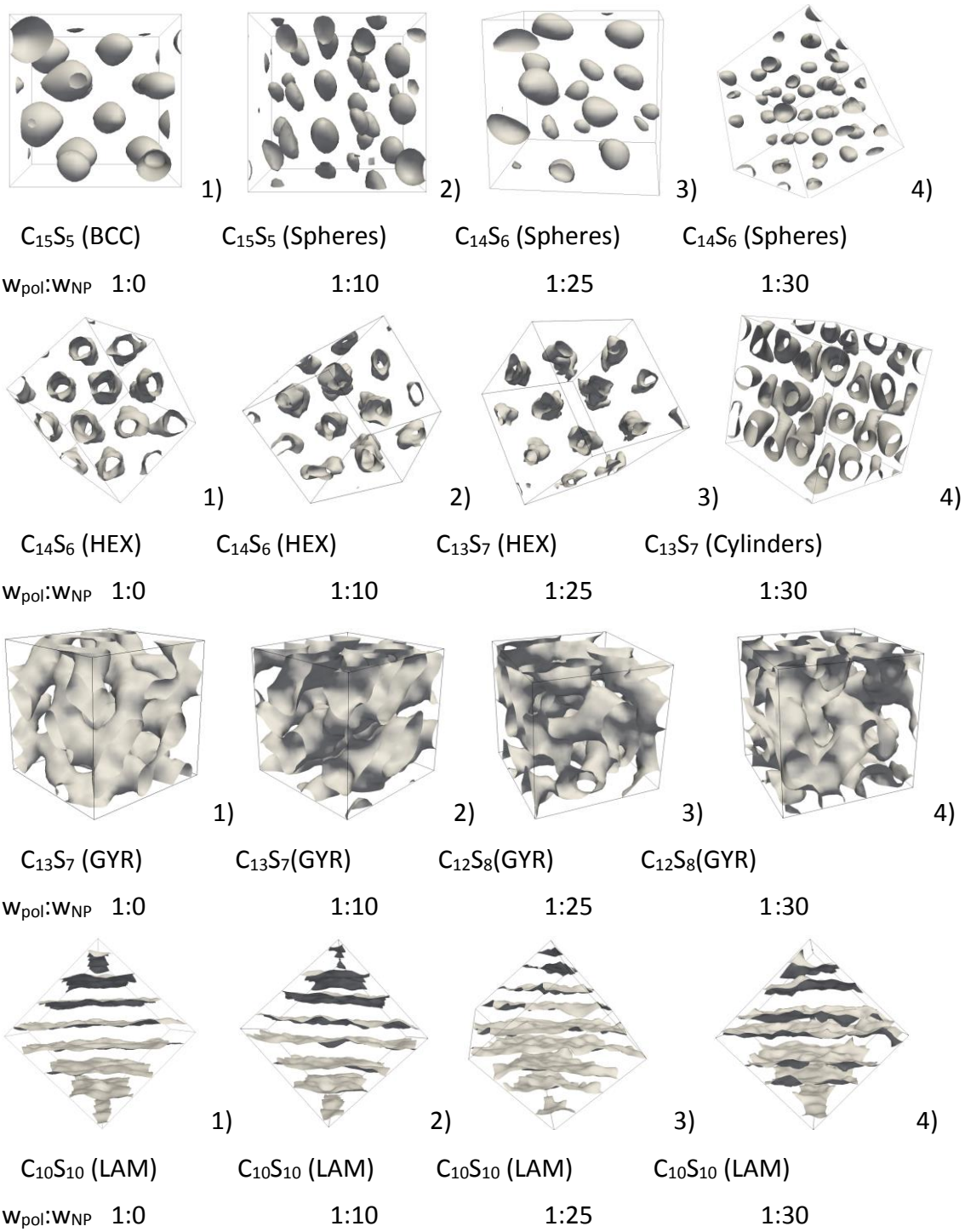

Figure ESI-2. Distibutions of S-beads for systems of $C_{15}S_5$, $C_{14}S_6$, $C_{13}S_7$, $C_{12}S_8$ and $C_{10}S_{10}$ chains having different w_{pol}:w_{NP} composition. The composition of copolymer chains, the content of NPs and the type of morphology are indicated under each picture. The isodensity surfaces for S particles correspond to the number densities larger than 1.4.

In Fig.ESI-2, the distibutions of S-beads are shown for systems of $C_{15}S_5$, $C_{14}S_6$, $C_{13}S_7$, $C_{12}S_8$ and $C_{10}S_{10}$ chains having different w_{pol}:w_{NP} composition. The type of morphology of S-beads distribution is indicated near each picture. One can see that with increasing of NP volume fraction in the simulation cell, the morphologies formed in pure copolymer system, such as HEX, GYR and LAM are significantly perturbed. However, for GYR morphology the bicontinuality along domains of both C- and S-blocks is still preserved, what has been checked using the clustering analysis is based on the algorithm from our previous work [1] (this point is discussed in this reference).

As regards the lamellar morphologies, they are well visible in pictures and most likely do not cause any doubt of readers. The gyroid morphologies are not so obvious, and therefore we have performed special analysis and have included its results in the paper. Here we present in Fig.ESI-3 and Fig.ESI-4 additional data on partial static structure factor $S_S(q)$ for S-blocks for cylindrical and spherical morphologies, including HEX and BCC structures.

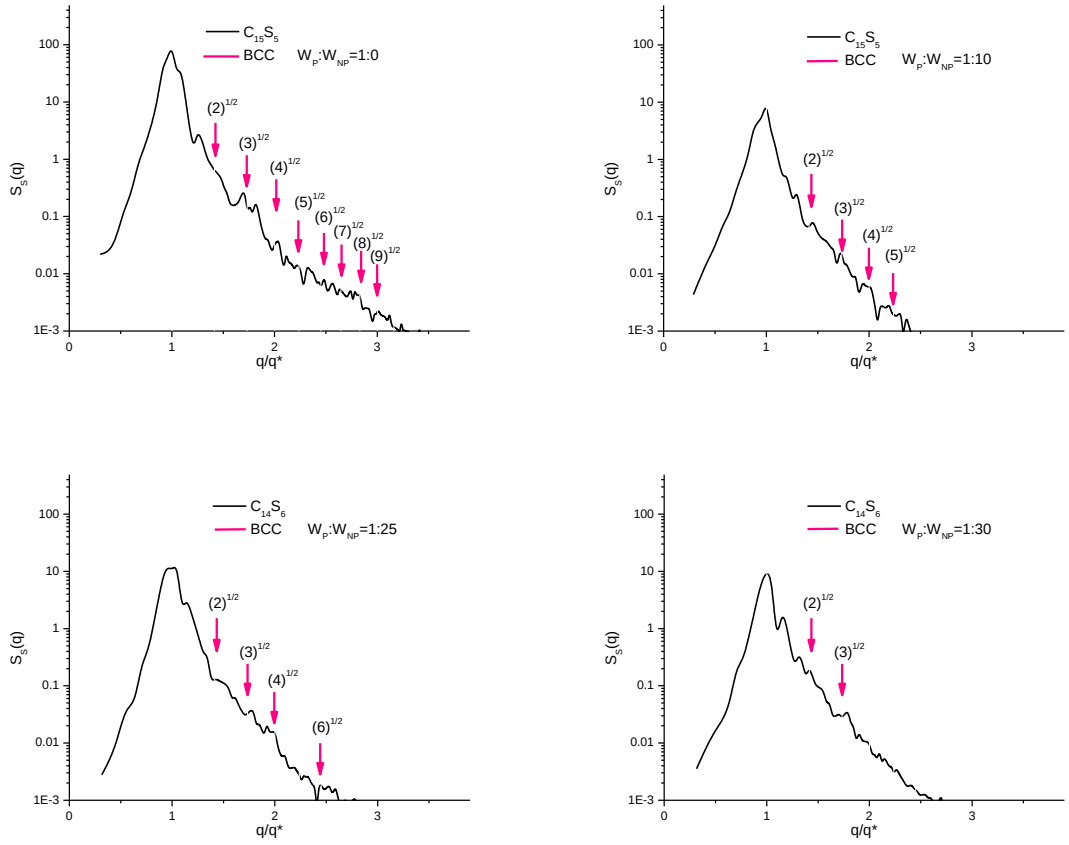

Figure ESI-3. Partial structure factor $S_S(q)$ for $C_{15}S_5$ (w_{pol}:w_{NP} =1:0), $C_{15}S_5$ (w_{pol}:w_{NP} =1:10), $C_{14}S_6$ (w_{pol}:w_{NP} =1:20) and $C_{14}S_6$ (w_{pol}:w_{NP} =1:30).

In Fig.ESI-3 we plot $S_S(q)$ for systems $C_{15}S_5$ (w_{pol} : w_{NP}=1:0), $C_{15}S_5$ (w_{pol} : w_{NP}=1:10), $C_{14}S_6$ (w_{pol} : w_{NP} = 1:20) and $C_{14}S_6$ (w_{pol} : w_{NP} = 1:30), and indicate in all plots the peaks at relative positions of 1: $2^{½}$: $3^{½}$: $4^{½}$: $5^{½}$: $6^{½}$: $7^{½}$ which would correspond to BCC structure [2]. With increasing the content of NPs, these peaks become much less pronounced. In the case of $C_{15}S_5$ (w_{pol} : w_{NP}=1:0) samples, the peaks are also not very well visible but their height is actually comparable with what is visible in real experiments [2]. This analysis of $S_S(q)$, as well as the visual analysis of snapshots in Fig.ESI-2 above, allows us to conclude that the BCC phase is present only in the case $C_{15}S_5$ (w_{pol} : w_{NP}=1:0) samples, but it smears out in systems with higher content of NPs, however, the spherical domains are preserved but are almost disordered.

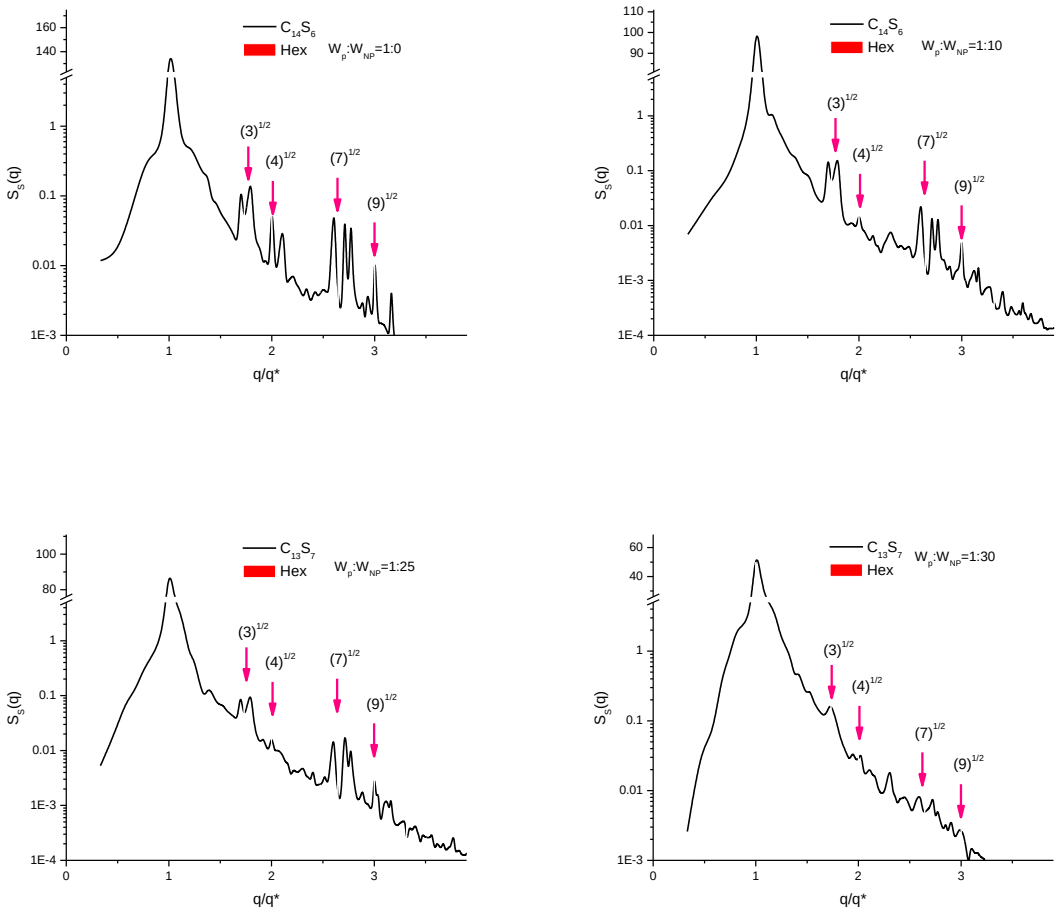

Figure ESI-4. Partial structure factor $S_S(q)$ for $C_{14}S_6$ (w_{pol} : w_{NP} = 1:0), $C_{14}S_6$ (w_{pol} : w_{NP} = 1:10), $C_{13}S_7$ (w_{pol}:w_{NP} = 1:25) and $C_{13}S_7$ (w_{pol} : w_{NP}=1:30).

In Fig.ESI-4 we plot $S_S(q)$ for systems $C_{14}S_6$ (w_{pol} : w_{NP} = 1:0), $C_{14}S_6$ (w_{pol} : w_{NP} = 1:10), $C_{13}S_7$ (w_{pol} : w_{NP} = 1:25) and $C_{13}S_7$ (w_{pol} : w_{NP} = 1:30) and indicate in all plots the peaks at relative positions of 1: $3^{½}$: $4^{½}$: $7^{½}$: $9^{½}$ which would correspond to HEX structure [2]. These data confirm that the samples for $C_{14}S_6$ (w_{pol} : w_{NP} = 1:0), $C_{14}S_6$ (w_{pol} : w_{NP} = 1:10) and $C_{13}S_7$ (w_{pol} : w_{NP} = 1:25) are in the HEX phase. In case $C_{13}S_7$ (w_{pol} : w_{NP} = 1:30) we observe perturbed cylinders (which even merge together in several places).

References:

[1] A.A. Markina, V.A. Ivanov, P.V. Komarov, A.R. Khokhlov, S.-H. Tung, *J. Phys. Chem. B*., 2017, 121, 7878-7888.

[2] Y.-Y.Huang, H.-L.Chen, T.Hashimoto, *Macromolecules*, 2003, 36, 764-770.